ISSN 0915-633X

NATIONAL INSTITUTE FOR FUSION SCIENCE

Rate Theory Modeling of Defect Evolution under Cascade Damage Conditions: The Influence of Vacancy-type Cascade Remnants and Application to the Defect Production Chracterization by Microstructural Analysis

Y. Katoh, T. Muroga, A. Kohyama, R.E. Stoller, C. Namba and O. Motojima

(Received - Oct. 27, 1995)

NIFS-386 Nov. 1995

RESEARCH REPORT
NIFS Series

NAGOYA, JAPAN

Rate Theory Modeling of Defect Evolution Under Cascade Damage Conditions: The Influence of Vacancy-type Cascade Remnants and Application to the Defect Production Characterization by Microstructural Analysis

Yutai Katoh[1*], Takeo Muroga[1], Akira Kohyama[2],
Roger E.Stoller[3], Chusei Namba[1] and Osamu Motojima[1]

[1] National Institute for Fusion Science, Nagoya 464-01, Japan
[2] Institute of Atomic Energy, Kyoto University, Uji, Kyoto 611, Japan
[3] Oak Ridge National Laboratory, Oak Ridge, TN 37831, USA
*E-mail: katoh@LHD.nifs.ac.jp

Abstract

Recent computational and experimental studies have confirmed that high energy cascades produce clustered defects of both vacancy- and interstitial-types as well as isolated point defects. However, the production probability, configuration, stability and other characteristics of the cascade clusters are not well understood in spite of the fact that clustered defect production would substantially affect the irradiation-induced microstructures and the consequent property changes in a certain range of temperatures and displacement rates. In this work, a model of point defect and cluster evolution in irradiated materials under cascade damage conditions was developed by combining the conventional reaction rate theory and the results from the latest molecular dynamics simulation studies. This paper provides a description of the model and a model-based fundamental investigation of the influence of configuration, production efficiency and the initial size distribution of cascade-produced vacancy clusters. In addition, using the model, issues on characterizing cascade-induced defect production by microstructural analysis will be discussed . In particular, the determination of cascade vacancy cluster configuration, surviving defect production efficiency and cascade-interaction volume is attempted by analyzing the temperature dependence of swelling rate and loop growth rate in austenitic steels and model alloys.

keywords:
irradiation effects, rate theory modeling, displacement cascade,
microstructural evolution, microstructural analysis

Introduction

Production of cascade vacancy clusters has long been observed in experiments[1-3] and demonstrated by computer simulation studies [4-6]. Generally, vacancy clusters are thermally stable at low to medium temperatures. Vacancy clusters, which are randomly introduced at very high production rates and possess a long lifetime, should impose great influences on point defect processes, microstructural evolution and resultant property changes in irradiated materials. Production of interstitial clusters in the periphery of cascade core regions is demonstrated by computer simulation studies as well [5-7]. Interstitial clusters in fcc metals appear to be very mobile and to move to sinks quickly under a stress field gradient in the defective lattice [8]. Modeling studies have shown this influences the partitioning of interstitial atoms to various kinds of sinks significantly in certain microstructural conditions [8-10]. However, in heavily irradiated materials where the sink density is very high, clustered interstitials tend to behave in a way similar to single interstitials do.

There have been some models of microstructural evolution in irradiated materials which include a description of cascade cluster evolution [11-14]. These models have been to some extent successful in assessing the effects of cascade vacancy cluster production qualitatively. However, recent molecular dynamics investigations of cascade defect production reveal that the initial size distribution of cascade vacancy clusters might be largely different from the assumption in those models [5,7]. In this work, a model of defect evolution in irradiated materials was developed, taking account of cascade vacancy cluster production in various manners according to the latest molecular dynamics simulation results. Using the developed model, the influences of cascade vacancy cluster production, configuration, clustering fraction and initial size distribution on the effective point defect flux and microstructural evolution were investigated.

Microstructural and microchemical changes as consequences of defect migration and accumulation are generally understood to be responsible for the irradiation-induced property degradation in fusion reactor materials. Therefore, the defect production characteristics and the effective flux of freely migrating point defects under cascade damage conditions are among the key issues to assess the materials behavior under fusion environment by mechanistic modeling. Attempts to clarify the defect production efficiency have been made for years both by experiments and computation. Computer simulations of cascade events by means of molecular dynamics has shown 10 to 20 percent of surviving defect fractions (SDF) in typical fcc metals at elevated temperatures [7,15,16]. SDF here is the number of cascade-produced Frenkel pairs, which survived in-cascade recombination by the end of the cascade cooling phase, relative to the number of displacements determined by the NRT definition. Since the produced defects are localized within or at the periphery of cascade core regions at the end of atomic process simulations, the SDF quoted above should be the maximum value of

the cascade-escaping defect fraction, which must be more or less smaller. Stochastic annealing simulations have provided some quantitative information on this issue [17,18], however, understanding of the effect of localized defect production is still insufficient. Results from the maximum swelling rate measurements are generally consistent with the calculated SDF at high temperatures, however, effective free defect production rates derived from other experiments including loop growth measurement [19,20] and radiation induced segregation [21] or radiation induced diffusion analyses [22] yielded to as low as several tenth percent. This discrepancy is most likely attributed to the effect of fine defect structures in part due to the complexity of defect production behavior particular to high energy cascade [23]. Such microstructural effect should influence swelling rates as well but have never been assessed systematically.

In the latter part of this paper, issues related to characterization of cascade-induced defect production by microstructural analysis, including swelling rate analysis in reactor-irradiated austenitic alloys and loop growth rate analysis in electron- and heavy ion-irradiated austenitic model alloy, are discussed.

Model description

Primary defect production

Computer simulation studies revealed the approximate number of Frenkel pairs produced by a certain energy recoil and the spatial distribution of defects at the end of the cascade cooling phase. This provides information on primary defect production such as defect production efficiency relative to NRT-dpa, clustered defect fractions and the cluster size distribution [24]. The effect of the spatial distribution of the defects relevant to high energy cascades, i.e., a vacancy rich region at the sub-cascade core surrounded by an interstitial-rich periphery, is not clear at present and therefore was not included in the current model. One affect of this distribution might be to reduce the escaping defect fraction.

From visual observation of the molecular dynamics simulation results in reference [7], the initial size distribution of cascade-produced vacancy clusters is fitted to exponential functions in this study. Then, the production rates of isolated vacancies and vacancy clusters are described as follows,

$$G_v(1) = G_{dpa}\eta(1-\chi) + \sum_j D_v C_v^j S_v^j \qquad (1)$$

$$G_v(j) = G_{dpa}\eta\chi \cdot \frac{\exp[p(j-1)]}{\sum_{k=2}^{N\max} \exp[p(k-1)]} \qquad (2)$$

where G_{dpa} is a displacement rate in dpa, η is a surviving defect fraction (SDF) relative to NRT-dpa, χ is a fraction of cascade-produced vacancies collapse into clusters (CDF_v), D_v is the vacancy diffusivity, C_v^j is the equilibrium vacancy concentration near sink classified j, S_v^j is the strength of the sink j, N_{max} is the maximum number of vacancies in cascade-produced clusters and p is a variable parameter which gives the initial size distribution of cascade vacancy clusters. The thermal emission term in equation (1) includes vacancy emission from small clusters such as di-vacancies or tri-vacancies. In the base case calculation N_{max} and the exponent p were set to 15 and -0.50, respectively, both of which were varied in a parametric analysis.

The in-cascade production of clustered interstitials was not included in this study. A preliminary calculation suggested that including interstitial clusters which migrate as easily as single interstitials does not significantly alter the defect flux when a high density of sinks exists. However, the influences of the production and mobility of interstitial clusters still need to be assessed for certain irradiation and material conditions.

Defect cluster evolution

Rate equations for concentration changes of vacancy clusters of individual sizes were formulated so that the influence of the initial cascade vacancy cluster size distribution could be seen. The time derivatives of vacancy and interstitial concentrations are expressed as follows,

$$\frac{dC_v}{dt} = G_v(1) - C_v\left(\sum_j D_v S_v^j + 2\alpha_v^v C_v + \sum_{j=2}^{Nv-1}\alpha_{jv}^v C_{jv} + \sum_{j=1}^{Ni}\alpha_{ji}^v C_{ji}\right) \quad (3)$$

$$\frac{dC_i}{dt} = G_i(1) - C_i\left(\sum_j D_i S_i^j + 2\alpha_i^i C_i + \sum_{j=2}^{Ni-1}\alpha_{ji}^i C_{ji} + \sum_{j=1}^{Nv}\alpha_{jv}^i C_{jv}\right) \quad (4)$$

where $G_i(1)$ is the isolated interstitial production rate including terms from small cluster evolution. N_v and N_i are the number of vacancies and interstitials, respectively, in the clusters of the largest size in the calculation. N_v and N_i are taken to be 500 and 50, respectively, in this study after confirming that replacing with significantly larger values do not affect the point defect concentrations. C_{jv} and C_{ji} are the concentrations of vacancy- and interstitial-clusters consisting of j defects. Their time derivatives are given below.

$$\frac{dC_{jv}}{dt} = G_v(j) + \alpha_{(j-1)v}^v C_{(j-1)v} C_v + C_{(j+1)v}\left[\alpha_{(j+1)v}^i C_i + \beta_{(j+1)v}\right] - C_{jv}\left(\alpha_{jv}^v C_v + \alpha_{jv}^i C_i + \beta_{jv}\right) \quad (5)$$

$$\frac{dC_{ji}}{dt} = G_i(j) + \alpha^{i}_{(j-1)i} C_{(j-1)i} C_i + C_{(j+1)i}\left[\alpha^{v}_{(j+1)i} C_v + \beta_{(j+1)i}\right] - C_{ji}\left(\alpha^{v}_{ji} C_v + \alpha^{i}_{ji} C_i + \beta_{ji}\right) \quad (6)$$

In equations (3) - (6), α and β are the rate constants for clustering and dissociation reactions which are given by combinatorial numbers, the vibrational frequency of the jumping defect, activation energy of the defect jump and the binding energy of the clusters [14,25]. Stable configurations of vacancy clusters in metals are usually found to be dislocation loops, voids or stacking fault tetrahedra (sft). The energies of such vacancy clusters have been derived by many authors. In this work, the energy expressions compiled by Zinkle, et al. [26] are used because of the validity to very small sizes. The base case parameters used in this study are summarized in table 1.

The objective of the current work is to clarify how the state of primary defect production influences the point defect flux. The point defect concentrations are essentially in equilibrium with a given microstructural condition because microstructural features such as grain boundaries, dislocations and cavities evolve much slower than the time constant for point defect concentration changes. Therefore, the steady-state solution was employed to calculate the defect concentrations.

Results and discussion

Influence of CVC configuration

The stability of vacancy clusters apparently depends very strongly on temperature, regardless of their configuration. At very high temperatures, cascade vacancy clusters disappear very quickly through emitting vacancies and consequently the cluster production does not affect the mean point defect flux in matrix. At very low temperatures, on the other hand, cascade vacancy clusters become the major site of point defect recombination and disappear mostly by the cascade-interaction. At intermediate temperatures, the behavior of vacancy clusters is determined by their configuration, or thermal stability, and interaction with migrating point defects.

Fig. 1 shows the temperature dependence of single point defect concentration with or without cascade vacancy cluster production. This figure also compares the influence of CVC production in different configurations, namely microvoids, faulted loops and stacking fault tetrahedra. The base case set of parameters were used for this calculation. Since the vacancy clusters produced by cascades are generally very small, combinatorial numbers for clustering or dissociation were assumed to be independent of cluster configuration. Therefore, the effects of cluster configuration here are solely through their thermal stability. The calculated effect of

CVC as faulted loops is close to that for the case of voids. This arises largely to the fact that the energy of very small loops (e.g., tri-vacancy, etc.) are replaced with the energy of the voids, because they are calculated unrealistically large by Kroupa's model [26]. Dislocation loops with a long range elastic field are often thought to possess significant interstitial bias and consequently have a much shorter life time compared to vacancy clusters in other configurations. However, it is hard to believe that very small vacancy clusters take such a high energy configuration that have a long range strain field when they can take other lower energy configurations.

In Fig. 2, the equivalent sink strength of the vacancy clusters is plotted against temperature, for the cases of no CVC production and CVC production as microvoids and sft. The vacancy cluster sink strength was estimated by the following equation.

$$S_v^{vcl} = \sum_{j=2}^{Nv-1}\left(\frac{\alpha_{jv}^{v} C_{jv}}{D_v}\right) \qquad (7)$$

When we compare the vacancy cluster sink strength with the typical dislocation sink strength in heavily irradiated austenitic steels, which is plotted together in Fig. 2, it might be noted that the influences of CVC production become significant when vacancy cluster sink strength is comparable with or greater than the dislocation sink strength, or more generally, sink strength of other microstructural defects which determine the properties of the material.

Fig. 3 compares the thermal lifetime and the irradiated lifetime, under a typical reactor-irradiation condition, relative to the thermal lifetime of a vacancy cluster in the form of microvoid or sft. Vacancy cluster size here was taken to be 10 vacancies. The irradiated life time appeared to be close to the thermal lifetime, or at the longest about 1.5 times of the thermal lifetime under typical microstructural conditions and no longer than 1.7 times of the thermal lifetime even under weak sink conditions where dislocation sink strength were taken to be 1/10 of the typical cases. This result leads to the following approximate guideline for the critical condition of a significant influence of cascade vacancy clusters,

$$S_v^{vcl} = \sum_{j=2}^{N\max}\left[\frac{\alpha_{jv}^{v} G_v(j)\tau_{jv}}{D_v}\right] \geq \rho_d \qquad (8)$$

where τ_{jv} is a thermal life time of vacancy clusters and ρ_d is a dislocation density.

Influence of clustered vacancy fraction

The fraction of cascade-produced vacancies which collapse into clusters (CDFv) is

one of the major points of interest. CDFv calculated by molecular dynamics typically falls around 0.6 but deviates by about ±0.1 to 0.2 [7]. The result of a calculation to see the effect of CDFv on point defect partitioning is shown in Figs. 4 A and B, in which the point defect recombination fractions in bulk, at vacancy clusters and at other sinks are plotted against CDFv. In the case of Fig. 4A, where the dislocation density was taken to be 10^{14} m^{-2}, vacancy cluster production by cascades reduces the defect flux to sinks only by small fractions even when CDFv is close to 1. The value of 10^{14} m^{-2} is close to but somewhat smaller than typical dislocation densities in irradiated austenitic stainless steels at this temperature.

In the Fig. 4B case, the dislocation density was taken to be 10^{13} m^{-2}. Although some austenitic model alloys exhibit an irradiated dislocation density as low as this, this artificial condition was chosen to demonstrate the influence of CDFv when it was expected to be most prominent within a 0.1 to 1.0 range. When CDFv is increased from 0.5 to 0.6, the point defect flux to sinks decreases by about 15 percent. The influence on CDFv on the temperature dependence of the swelling rate is calculated for the cases that cascades produce microvoids or sft and shown in Fig. 5. This result confirms that major differences in CDFv in the vicinity of 0.5 might alter the swelling rate only by small fractions.

Influence of initial CVC size distribution

In conventional rate theory models including cascade vacancy cluster evolution, it has been assumed that clusters of an average size (N) are produced at the rate equal to $G_{dpa} \cdot \eta \cdot CDFv / N$ [11-14]. Such an assumption apparently overestimates the average stability of clusters, therefore, it is important to know how a more practical initial size distribution influences the results. Fig. 6A compares the temperature dependence of the swelling rate when the initial size distribution of cascade vacancy clusters follows equation (2) and cascade clusters consisting of 10 vacancies are exclusively produced. In the latter case, the suppression of free defect concentration occurs from higher temperatures. The temperature dependence shift of average sink strength of vacancy clusters, which appears as a swelling rate suppression in Fig. 6A, had a different implication in swelling rate analysis in a previous work [27] and the current study.

In Fig. 6B, the effect of the maximum size of cascade-produced vacancy clusters and the exponent in the size distribution function, expressed as N_{max} and p in equation (2), respectively, on swelling rate is presented. In this analysis, temperature and cluster configuration were chosen to be 723K and stacking fault tetrahedron so that the influence of an average cluster stability could clearly be seen. The result shows that, in general, N_{max} greater than 10 imposes only a very small influence on defect flux to sinks unless p is close to 0. Therefore, from the viewpoint of microstructural evolution, production of large vacancy clusters at relatively small probability is not very important. On the other hand, the value of p

affects the free defect flux significantly. As shown in the inset to Fig. 6B, decreasing p by 0.25 increases the production rate of 12-vacancy clusters by about 10 times, and this sensitivity is mostly responsible for the defect flux changes. p is expected to positively correlate with the damage energy of the primary knock-on atoms, though molecular dynamics simulation results so far do not clearly exhibit such a tendency [7].

Defect production characterization by swelling rate analysis

As discussed in the previous sections, the most apparent effect of cascade cluster production on microstructural evolution is through suppression of free defect flux to sinks. Analyzing swelling rate is a quick way to characterize the defect production, because (1) swelling rate is proportional to the free defect flux to sinks, (2) swelling rate is an averaged measure of defect partitioning between different kinds of sinks, therefore localized fluctuation of defect flow can be ignored, (3) swelling rate can be measured as a function of irradiation temperature with relatively small uncertainty, and (4) considerable amount of experimental data have been accumulated especially for austenitic alloys. On the other hand, negative issues include uncertainty of dislocation-interstitial bias, the roll of precipitates, the roll of other defects which are invisible by ordinary microstructural examination represented by transmission electron microscopy.

Data of swelling rate in austenitic steels and model alloys from reactor irradiation experiments are summarized in table 2 [28-34]. Swelling rates were derived assuming linear swelling when not provided in literature. Therefore, swelling rates might be somewhat underestimated in case number of data points were insufficient. It should be noted that in many cases core components of fast reactors exhibit significantly larger swelling than the identical material does in material irradiation experiments, probably due to the effects of stress field and complex irradiation history. In table 2, supplemental microstructural data are attached when available. The $4\pi N_c r_c$ column corresponds to cavity sink strength, ignoring multiple-sink correction factors. Dislocation sink strength, according to formulation in reference [35], typically falls to 1 ~ 2 times of the dislocation line density. This factor tends to increase with the increasing dislocation density. However, assumed homogeneous dislocation distribution underestimates the effective mean dislocation spacing and consequently overestimates dislocation sink strength under high dislocation density conditions where spatial distribution of dislocations is considerably inhomogeneous. Therefore, in this study, dislocation sink strength is assumed to be equal to the line density. From the general trend in table 2, dislocation density and cavity number density are assumed to follow the temperature dependence below.

$$\rho_d(m^{-2}) = 2.32 \times 10^{18} \cdot \exp[-0.0115T(K)] \qquad (9)$$

$$N_c(m^{-3}) = 1.35\times10^{28}\cdot\exp[-0.023T(K)] \qquad (10)$$

The model used in this study is based on a comprehensive model of microstructural evolution developed by Katoh, Stoller and Kohyama [36] but modified to include cascade cluster production in more complex manner. SDF, clustered vacancy fraction (CDFv), maximum cascade vacancy cluster size (N_{max}) and the exponent of size distribution function (p) are taken as 0.15, 0.65 times SDF, 15 and -0.5, respectively, unless otherwise noted. Stacking fault tetrahedra, microvoids and faulted dislocation loops were considered as a possible vacancy cluster configuration. Energy expression of vacancy clusters in reference [26] was used, but reduced surface energy was employed on microvoid energy calculation to account for the effect of indefinite surface of very tiny void.

The calculated temperature dependence of swelling rate under sink conditions described above, which are typical in austenitic steels heavily irradiated in reactors, is shown in Fig. 7 for the cases of no cascade vacancy cluster (CVC) production (i.e., CDFv = 0) and CVC's make microvoids, faulted loops or sft. Under dense sink conditions used in this set of calculation, major part of free point defects annihilate at sinks even at the lowest temperature here or 623 K. Therefore, swelling rate when cascades do not produce clusters is determined mostly by relative sink strength of cavities, biased dislocations and grain boundaries. The reason for the reduced swelling rate at lower temperatures in the no CVC case is the increased dislocation sink strength relative to that of cavities'. Similarly, at high temperatures swelling rate also decreases slightly due to increased contribution of grain boundaries. Swelling rate is likely to be significantly influenced by the grain size at above 773 K under typical range of grain sizes in austenitic stainless steels. The influence of CVC production appears as a steep drop of swelling rate below a certain temperature. The criteria for this swelling suppression is discussed before. The current model ignores the effect of cascade overlapping on vacancy cluster evolution. Including such effect should make the slope less inclined at low temperatures.

The swelling rate data summarized in table 2 are plotted together in Fig. 7. The experimental data points and hatches generally fall below the calculated 'no CVC' curve below 723K and the discrepancy tends to enlarge with the decreasing temperature. This trend of temperature dependence is consistent with the model calculation considering CVC production as sft. Vacancy clusters should relax into the most stable form, namely sft in this case, before long time at elevated temperatures. However, vacancy clusters of only limited sizes, such as 3-v, 6-v, 10-v and 15-v, can take a perfect sft configuration and so the clusters of other sizes have larger energy than of perfect sft even if they take similar morphologies. The fact that the data points / hatches in Fig. 7 scatter around the calculated 'sft' curve but in

general somewhat biased toward 'loop' or 'microvoid' side except for the abnormally low-swelling cases suggests that cascade vacancy clusters of relatively large sizes transform into sft or similar lowest energy configurations, depending on their sizes, within their early life period.

Besides complex effect of microstructures, difficulties in quantitative discussion on swelling rate reside in that swelling rate in ideal conditions is determined by the product of two unknown factors, namely SDF and bias factor. In Figs. 8A and B, the influences of SDF and bias factor z on temperature dependence of swelling rate with or without CVC production are shown, respectively. In this paper, z is defined as sink strength of dislocations against interstitials relative to that against vacancies.

$$z = \frac{S_d^i}{S_d^v} \qquad (11)$$

From this calculation, it is obvious that any combination of SDF and z within their reasonable ranges can not explain the experimentally obtained trend of temperature dependence of swelling rate.

It should also be noted that, in case cascades produce vacancy clusters, the influences of SDF and z in Figs. 8A and B are apparently unlike. This is because the relationship between swelling rate, SDF and z described above is not valid any more when CVC's consume significant fraction of point defects which otherwise go to dislocations or cavities. When SDF is increased, swelling rate suppression due to vacancy clusters occurs below higher temperature, because the CVC production rate is proportional to SDF. Meanwhile, practically z does not affect the CVC evolution and simply contribute to swelling rate regardless of temperature. Therefore, SDF and z may possibly be determined separately when the nature and behavior of CVC are well understood.

The calculated relationship between swelling rate, SDF and z when no cascade clusters are produced is shown in Fig. 9. In this calculation, temperature of 773 K was chosen so that experimentally obtained swelling rate is not significantly influenced by either cascade clusters or grain boundaries. Although effective z may vary depending on sink conditions, temperature and solute segregation, very small SDF as low as a few percent derived from some experiments requires unrealistic large z, when several tenth percent per dpa of swelling rates are observed even in almost precipitates-free model austenitic alloys.

Cascade damage characterization by loop growth measurement

Growth rate of dislocation loops could be another measure of the free defect flux. Frank loops as interstitial clusters hardly emit interstitials or vacancies at temperatures they

can nucleate through free defect clustering. Therefore, radial growth rate of a faulted loop of interstitial type in fcc metals is written as

$$\frac{dr_l}{dt} = \frac{1}{b}\left(z_l^i D_i C_i - z_l^v D_v C_v\right) \qquad (12)$$

where b is Burger's vector magnitude and $z_l^{i,v}$ are the bias factors. Assuming the bulk dominating condition during early stages of microstructural development in annealed materials, relative production rate of freely migrating point defects can simply be derived by loop growth rate comparison [20]. In this approach, in spite of the advantage that experiments could be done in a well defined experimental environment, the influence of cascade cluster production has to be clarified to validate the result, because a build-up of cascade vacancy clusters occurs in low temperature and high displacement rate conditions in experiments for this purpose.

The model used for loop growth analysis is essentially same as that used in swelling rate analysis. Loop number density was given as an external parameter.

$$N_l(m^{-3}) = 1.24 \times 10^{32} \cdot \exp\left[-0.0345T(K)\right] \qquad (13)$$

Since the effect of cascade overlapping is not modeled here, equilibrium vacancy cluster concentration becomes unrealistically high under certain combinations of displacement rate and temperature. In such cases, calculation was terminated as soon as the total concentration of vacancy clusters reached 10^{-5} and point defect concentrations at that moment were regarded as those in steady-state.

Calculated effect of cascade characteristics, namely reduced SDF and vacancy cluster production, on temperature dependence of loop growth rate at displacement rates of 10^{-6} dpa/s and 10^{-4} dpa/s are shown in Figs. 10A and B, respectively. SDF is actually a relative damage rate, hence the loop growth rate is proportional to $SDF^{1/2}$ ~ SDF^{1} depending on irradiation and sink conditions, except for high temperature cases. Effect of CVC production is more sensitive to temperature than observed in the swelling rate analysis. At the damage rate of 10^{-4} dpa/s, saturation of vacancy cluster concentration is observed below about 700K. Therefore, it should be reasonable to understand that observed loop growth rate differences in 1MeV electron and 4MeV Cu ion irradiation experiments represent the effects of SDF and saturated vacancy cluster concentration under a cascade-overlapping condition.

In Fig. 11, calculated relationship between loop growth rate and saturated vacancy cluster concentration at 623K and 10^{-4} dpa/s is presented. The point at which loop growth rate starts decreasing shows the approximate concentration of vacancy clusters when their sink

strength is comparable with the loop sink strength. In reference [20], loop growth rate in 4MeV Cu ion irradiation experiment was in average about 1/10 of that in electron irradiation. When SDF is assumed to be 0.15 for the Cu ion case, contribution of the SDF difference should be about 0.4, and therefore the rest 0.25 might be attributed to the effect of vacancy clusters. Vacancy cluster concentration in this case is estimated from the following relationship,

$$\frac{1}{3}\cdot\frac{z_{vcl}}{a_o^2}\cdot C_{vcl}^{*} = 2\pi\, r_l\, N_l \qquad \cdot\ (14)$$

where z_{vcl} is the averaged combinatorial number of vacancy clusters with point defects and a_o is the lattice parameter. Estimating the loop sink strength to be about 10^{15} m^{-2} from microstructural information, and assuming $z_{vcl} = 10^2$, the vacancy cluster concentration yields to $C^{*}_{vcl} \cong 4\times10^{-6}$. Meanwhile, when CVC's annihilate only by cascade-overlapping, saturated vacancy cluster concentration is determined as follows.

$$\overline{C}_{vcl} = \frac{G_{vcl}}{G_{sc}V_{sc}} \qquad (15)$$

Here, G_{vcl} is a vacancy cluster production rate, G_{sc} is a sub-cascade production rate and V_{sc} is a mixing volume per sub-cascade. From the relationship below,

$$\frac{G_{vcl}}{G_{sc}} = \frac{\overline{N}_{FP}^{sc}}{\overline{N}_{v}^{cvc}} \qquad (16)$$

the condition $\overline{C}_{vcl} = 4\times10^{-6}$, $\overline{N}_{FP}^{sc} = 10$ (average number of Frenkel pairs per sub-cascade), $\overline{N}_{v}^{cvc} = 3.0$ (average number of vacancies in CVC) leads to a sub-cascade interaction radius,

$$r_{sc} = \left(\frac{3V_{sc}}{4\pi}\right)^{1/3} \cong 58\ \left(\Omega^{1/3}\right)$$

where Ω is an atomic volume. Assuming sub-cascade damage energy (T_{sc}) of 30keV (26keV and 33keV of damage energy per sub-cascade calculated by binary collision approximation are reported for Cu and Fe, respectively [37]), derived r_{sc} is somewhat larger than, or about 1.7 times, the outer radius of interstitial cluster shell, empirically derived as $r(a_o) \cong 7\left[T_{sc}(keV)\right]^{1/3}$ from molecular dynamics simulations by Foreman, et al. [38], where significantly high transient interstitials flux during the cascade event is expected. The

discrepancy could be attributed to difference of interaction radius and interstitial cluster shell radius, difference in damage energy in molecular dynamics simulation used as a model basis, ignored mobility of small vacancy clusters or insufficient understanding of cascade interaction behavior. However, the result of this comparison supports the implication that free defect flux is determined by the vacancy cluster concentration saturated by cascade interaction.

Conclusions

A model of point defect and cluster evolution in irradiated materials was developed by combining conventional reaction rate theory and results from the latest molecular dynamics simulation studies. Using the developed model, influences of configuration, production efficiency and initial size distribution of cascade-produced vacancy clusters were first investigated, and then determination of cascade-produced defect characteristics, such as surviving defect production efficiency and cascade cluster configuration, was attempted by means of swelling and loop growth analysis.

It was shown that point defect flux is largely influenced by the production of cascade vacancy clusters in stable configurations, and the criterion for significant influence by vacancy clusters was provided in terms of equivalent sink strength. The calculation also showed that point defect flux is not sensitive to the clustered fraction of cascade-produced vacancies but to the initial cluster size distribution, especially to a parameter in the exponential size distribution function. Understanding the correlation of such defect production parameters with the damage energy spectrum will be helpful for studies on the effect of neutron energy spectra.

An investigation on the temperature dependence of swelling suggested that CVC in austenitic alloys relax into stacking fault tetrahedra or similar lowest energy configurations during their early life and then act as effective sinks of point defects below a certain temperature. Effects of surviving defect fraction and dislocation-interstitial bias on temperature dependence of swelling rate appeared dissimilar when CVC effect was significant. The loop growth rate analysis showed that the CVC production is likely to be the major cause of the rate suppression at relatively low temperatures. Steady-state vacancy cluster concentration was estimated from the analysis, and the contribution of cascade-overlapping was discussed in terms of cascade interaction radius.

References

[1] R.S.Averback, K.L.Merkle and L.J.Thompson, Radiation Effects 51 (1980) 91.

[2] M.A.Kirk, I.M.Robertson, M.L.Jenkins, C.A.English, T.J.Black and J.S.Vetrano, J.Nucl.Mater. 149 (1987) 21.

[3] R.Rauch, J.Peisl, A.Schmalzbauer and G.Wallner, J.Nucl.Mater. 168 (1989) 101.

[4] H.L.Heinisch, J.Nucl.Mater. 117 (1983) 46.

[5] C.A.English, W.J.Phythian and A.J.E.Foreman, J.Nucl.Mater. 174 (1990) 135.

[6] T.Diaz de la Rubia and M.W.Guinan, Mater.Sci.Forum 97-99 (1992) 23.

[7] W.J.Phythian, R.E.Stoller, A.J.E.Foreman, A.F.Calder and D.J.Bacon, J.Nucl.Mater. 223 (1995) 245.

[8] H.Trinkaus, B.N.Singh and A.J.E.Foreman, J.Nucl.Mater. 199 (1992) 1.

[9] C.H.Woo and B.N.Singh, Phil.Mag.A 65 (1992) 889.

[10] B.N.Singh and A.J.E.Foreman, Phil.Mag. A 66 (1992) 975.

[11] R.E.Stoller and G.R.Odette, ASTM STP 782 (1982) 275.

[12] R.E.Stoller and G.R.Odette, ASTM STP 955 (1987) 371.

[13] Y.Katoh, R.E.Stoller, Y.Kohno and A.Kohyama, J.Nucl.Mater. 210 (1994) 290.

[14] Y.Katoh, R.E.Stoller and A.Kohyama, J.Nucl.Mater. 212-215 (1994) 179.

[15] H.Hsieh, T.Diaz de la Rubia, R.S.Averback and R.Benedek, Phys.Rev. B 40 (1989) 9986.

[16] C.A.English, A.J.E.Foreman, W.J.Phythian, D.J.Bacon and M.L.Jenkins, in Materials Modeling: From Theory to Technology, C.A.English, J.R.Matthews, H.Rauh, A.M.Stoneham and R.Thepford, Eds., Institute of Physics Publications, Bristol (1992) 105.

[17] T.Muroga, Radiat.Eff.Def.Solids 113 (1990) 119.

[18] H.L.Heinisch, Radiat.Eff.Def.Solids 113 (1990) 53.

[19] T.Kimoto, C.W.Allen and L.E.Rehn, J.Nucl.Mater. 191-194 (1992) 1194.

[20] T.Muroga, K.Mihara, H.Watanabe and N.Yoshida, J.Nucl.Mater. 212-215 (1994) 203.

[21] L.E.Rehn, P.R.Okamoto and R.S.Averback, Phys.Rev. B 30 (1984) 3073.

[22] V.Naundorf, M.-P.Macht and H.Wollenberger, J.Nucl.Mater. 186 (1992) 227.

[23] L.E.Rehn and H.Wiedersich, Mater.Sci.Forum 97-99 (1992) 43.

[24] S.J.Zinkle and B.N.Singh, J.Nucl.Mater. 199 (1993) 173.

[25] R.A.Johnson, J.Nucl.Mater. 83 (1979) 147.

[26] S.J.Zinkle, L.E.Seitzman and W.G.Wolfer, Phil.Mag.A 55 (1987) 111.

[27] Yutai Katoh and Akira Kohyama, Nucl.Inst.Meth. B 102 (1995) 12.

[28] Y.Katoh, Y.Kohno and A.Kohyama, J.Nucl.Mater. 212-215 (1994) 464.

[29] F.A.Garner, K.Miyahara, J.W.Newkirk and H.Kinoshita, J.Nucl.Mater. 199 (1993) 132.

[30] B.J.Makenas, ASTM STP 955 (1987) 146.

[31] I.Shibahara, N.Akasaka and S.Onose, to be published in ASTM STP 1270 (1995).

[32] R.E.Stoller, Microstructural Evolution in Fast-Neutron-Irradiated Austenitic Stainless Steels, ORNL-6430 (1987)

[33] M.Suzuki, S.Hamada, P.J.Maziasz, M.P.Tanaka and A.Hishinuma, ASTM STP 1046 (1989) 160.

[34] S.Hamada, M.Suzuki, P.J.Maziasz, A.Hishinuma and M.P.Tanaka, ASTM STP 1046 (1989) 172.

[35] A.D.Brailsford and R.Bullough, Philos.Trans.Roy.Soc.London 302 (1981) 87.

[36] Y.Katoh, R.E.Stoller, Y.Kohno and A.Kohyama, J.Nucl.Mater. 210 (1994) 290.

[37] H.L.Heinisch and B.N.Singh, Phil.Mag. A 67 (1993) 407.

[38] A.J.E.Foreman, W.J.Phythian and C.A.English, Phil.Mag. A 66 (1992) 671.

	value	unit
Irradiation parameters:		
Displacement rate	10^{-6}	dpa/s
Surviving defect fraction	0.15*	
Clustered vacancy fraction	0.65*	
Maximum CVC size	15*	
CVC size distribution function exponent (see text)	-0.50*	
Material parameters:		
Vacancy diffusivity pre-exponential	5×10^{-5}	m^2/s
SIA diffusivity pre-exponential	5×10^{-6}	m^2/s
Vacancy formation energy	1.50	eV
Vacancy migration energy	1.40	eV
SIA migration energy	0.85	eV
Di- and Tri-interstitial binding energy	1.35, 1.75	eV
Lattice parameter	3.56×10^{-10}	m
Dislocation-interstitial bias factor	1.10	
Stacking fault energy	4×10^{-2}	J/m^2
Surface free energy	$1.0 - 1.8 \times 10^{-3} \times (T-773)$	J/m^2

* Base case parameters. Varied in parametric analysis.

Tab. 1 - List of parameters.

Experiment	Temperature	Swelling rate(%/dpa)	ρ_d (m^{-2})	$4\pi N_c r_c$ (m^{-2})
JPCA-SA [28]	663K	0.011	2.4×10^{15}	1.5×10^{14}
(FFTF/MOTA)	683K	0.026	2.6×10^{15}	3.7×10^{14}
	733K	0.008	9.6×10^{14}	1.8×10^{13}
	793K	0.33	7.2×10^{14}	3.3×10^{13}
JPCA-CW [28]	663K	0.0024	2.5×10^{15}	3.0×10^{13}
(FFTF/MOTA)	683K	0.020	2.2×10^{15}	3.2×10^{14}
Fe-15Cr-25Ni[29]	727K	0.04~0.08	N/A	N/A
(EBR-II)	755K	0.02~0.05	N/A	N/A
	783K	0.03~0.05	N/A	N/A
316SS-CW[30]	708~753K	0.1~0.2	N/A	N/A
(FFTF)	753~763K	0.2~0.4	N/A	N/A
	763~853K	0.2~0.7	N/A	N/A
Fe-15Cr-20Ni[31]	749K	0.4	1.4×10^{14}	2.3×10^{14}
(JOYO)	845K	0.7	6.6×10^{13}	3.2×10^{13}
	894K	0.01	1.1×10^{13}	2.1×10^{13}
316SS-CW[31]	749K	0.005	3.1×10^{14}	7.2×10^{13}
(JOYO)	845K	0.1	4.3×10^{13}	3.9×10^{12}
	894K	0.04	2.8×10^{13}	1.0×10^{12}
316SS-CW[32]	650~692K	0.1~0.3	N/A	N/A
(FBRs)	717~758K	0.4~0.8	N/A	N/A
	782~835K	0.3~0.8	N/A	N/A
JPCA-SA[33] (HFIR)	773K	0.14	N/A	N/A
316SS-SA[34]	673K	0.01	5.7×10^{14}	1.0×10^{15}
(HFIR)	773K	0.05	2.0×10^{14}	1.1×10^{14}

N/A: Not available

Tab. 2 - Data on swelling rate of austenitic steels and model alloys from reactor irradiation experiments.

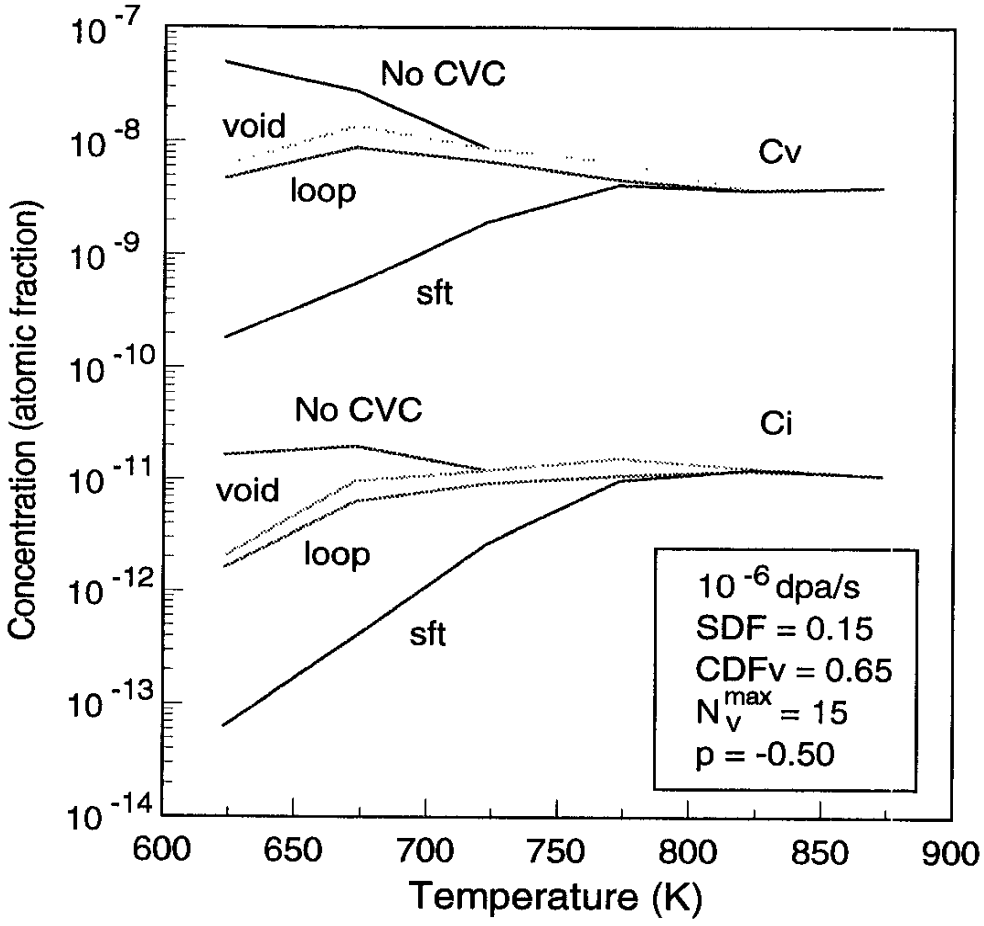

Fig. 1 - Influence of cascade vacancy cluster production and vacancy cluster configuration on temperature dependence of isolated point defect concentration.

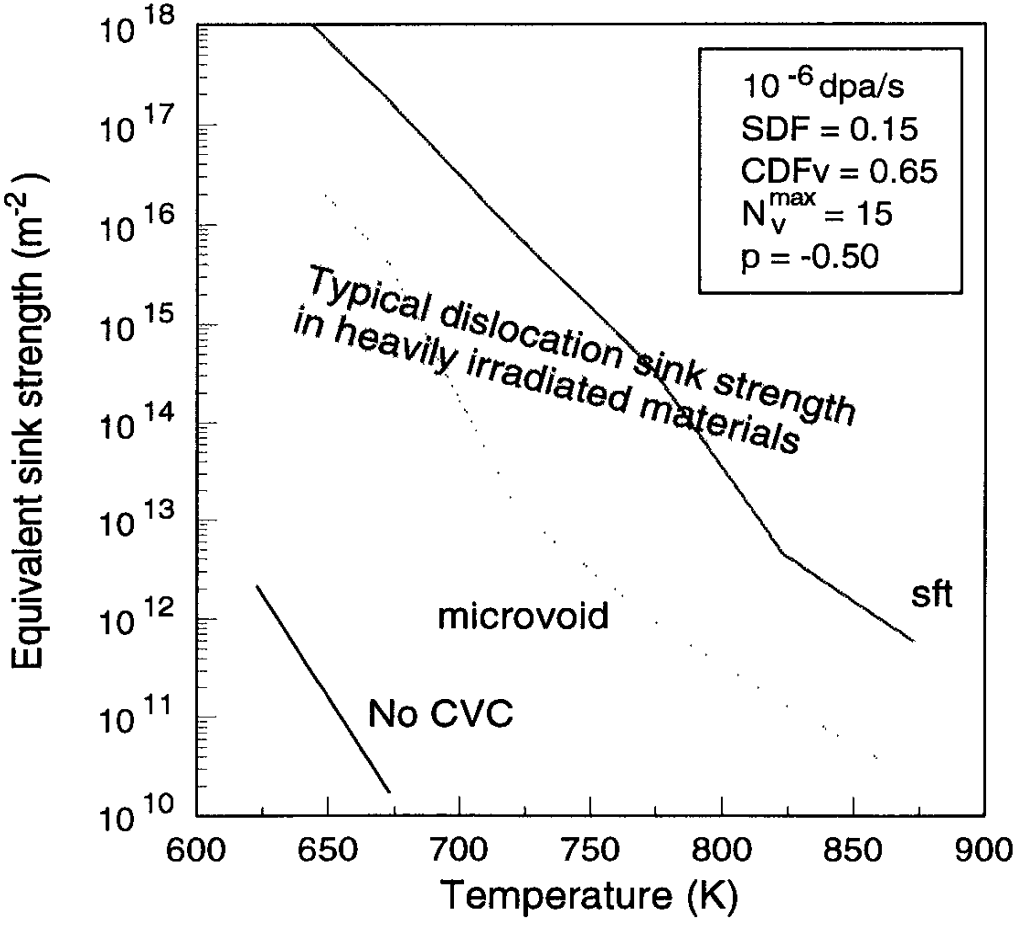

Fig. 2 - Estimated equivalent sink strength of vacancy clusters as a function of temperature with or without cascade vacancy cluster production.

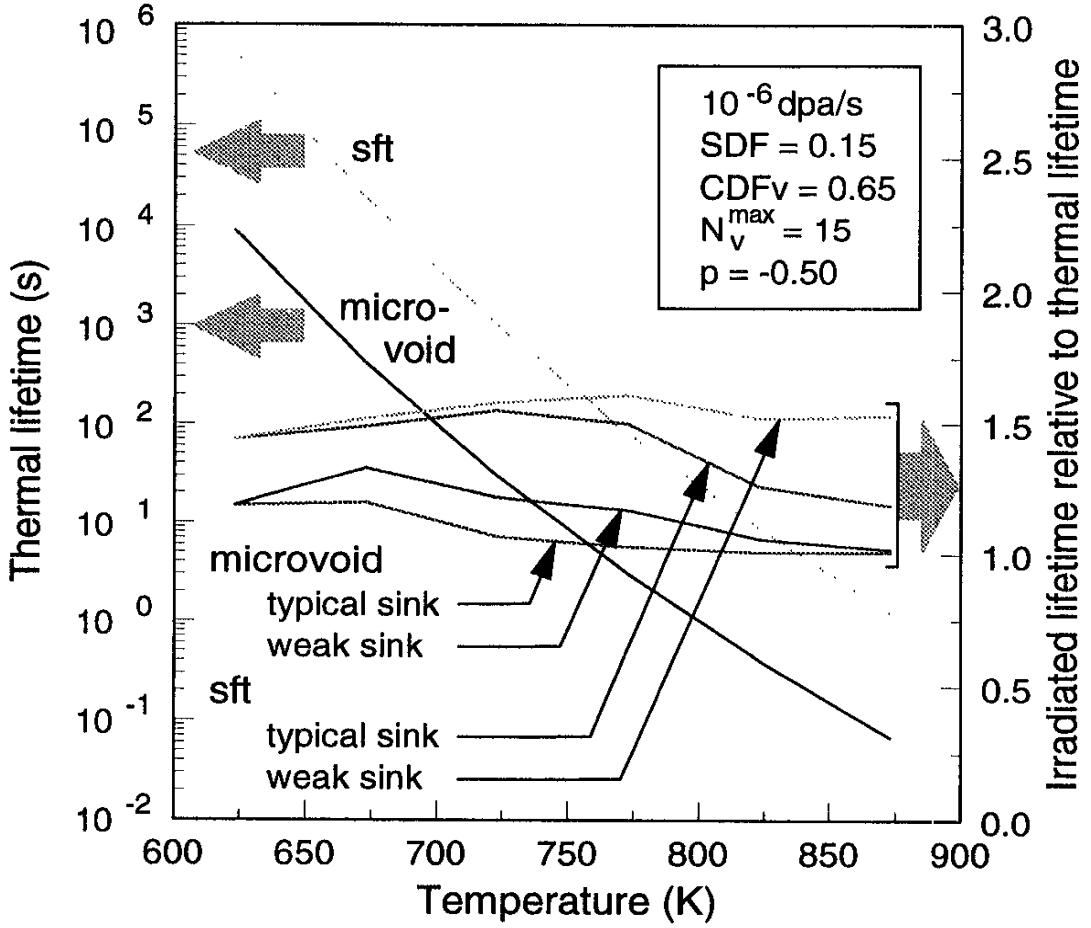

Fig. 3 - Calculated stability of a vacancy cluster as a microvoid or stacking fault tetrahedron according to the energy description used in this study: temperature dependence of thermal lifetime and irradiated lifetime relative to the thermal lifetime under typical and weak sink conditions. Vacancy cluster size was taken to be 10 vacancies. Weak sink strength was set equal to one tenth of the typical sink strength.

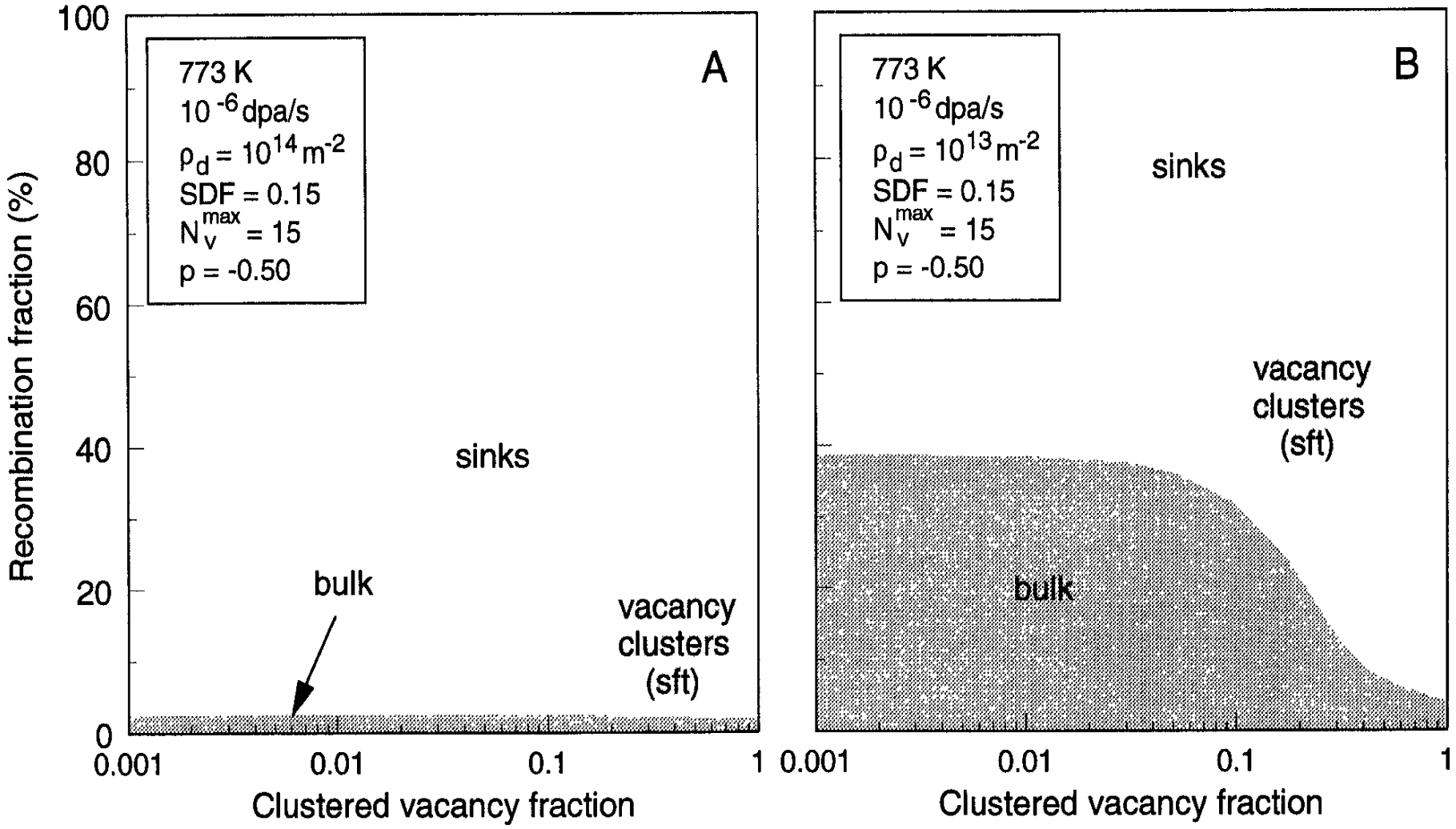

Fig. 4 - Estimated dependecne of partitioning of freely migrating point defects on clustering fraction of cascade-produced vacancies. The label `bulk' represents the fraction of vacancy flux to single interstitials and interstitial clusters. Under typical microstructural conditions in heavily irradiated materials (A), clustered vacancy fraction exerts only small influence on point defect flux to sinks. When dislocation sink strength is very weak, large difference in clustered vacancy fraction may result in possibly meaningful change in defect flux to sinks.

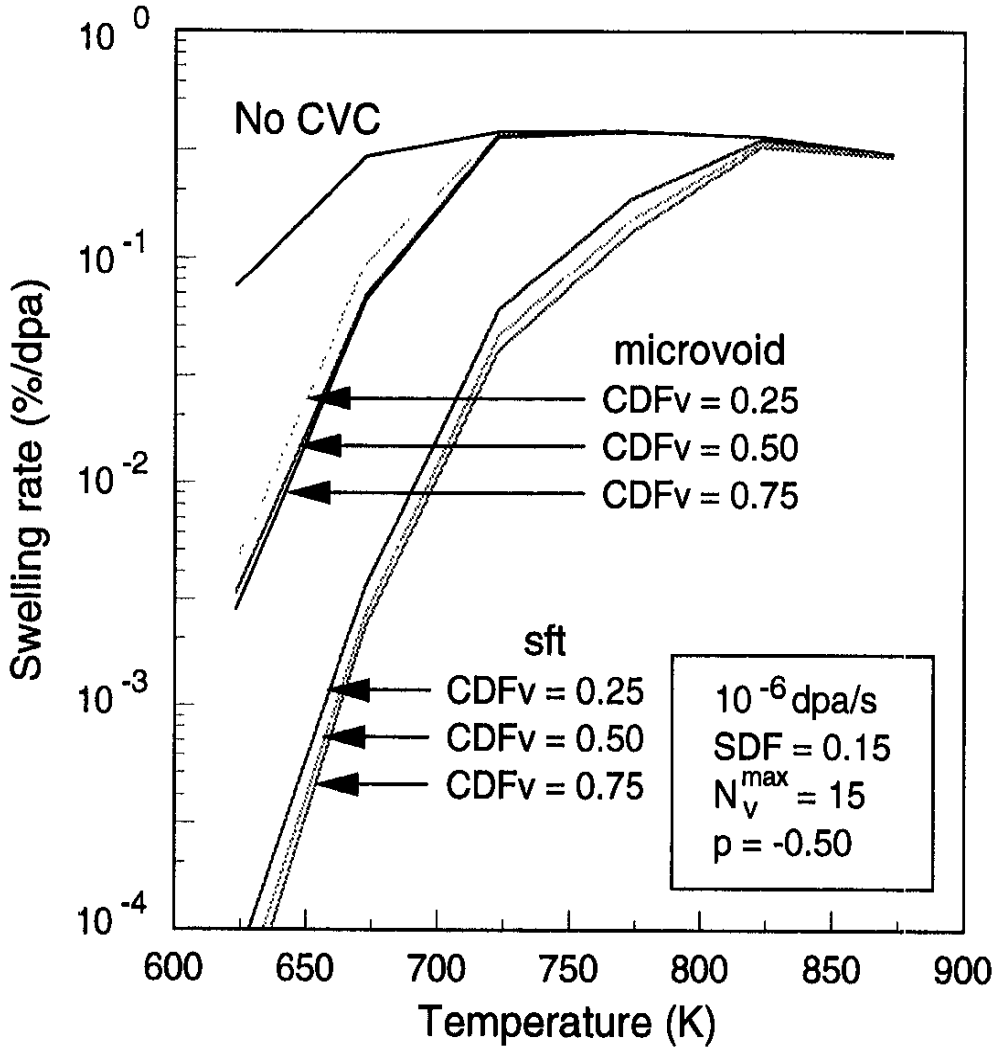

Fig. 5 - Influcence of clustered fraction of cascade-produced vacancies on temperature dependence of swelling rate under microstructural conditions typical in heavily irradiated austenitic steels at the given temperatures.

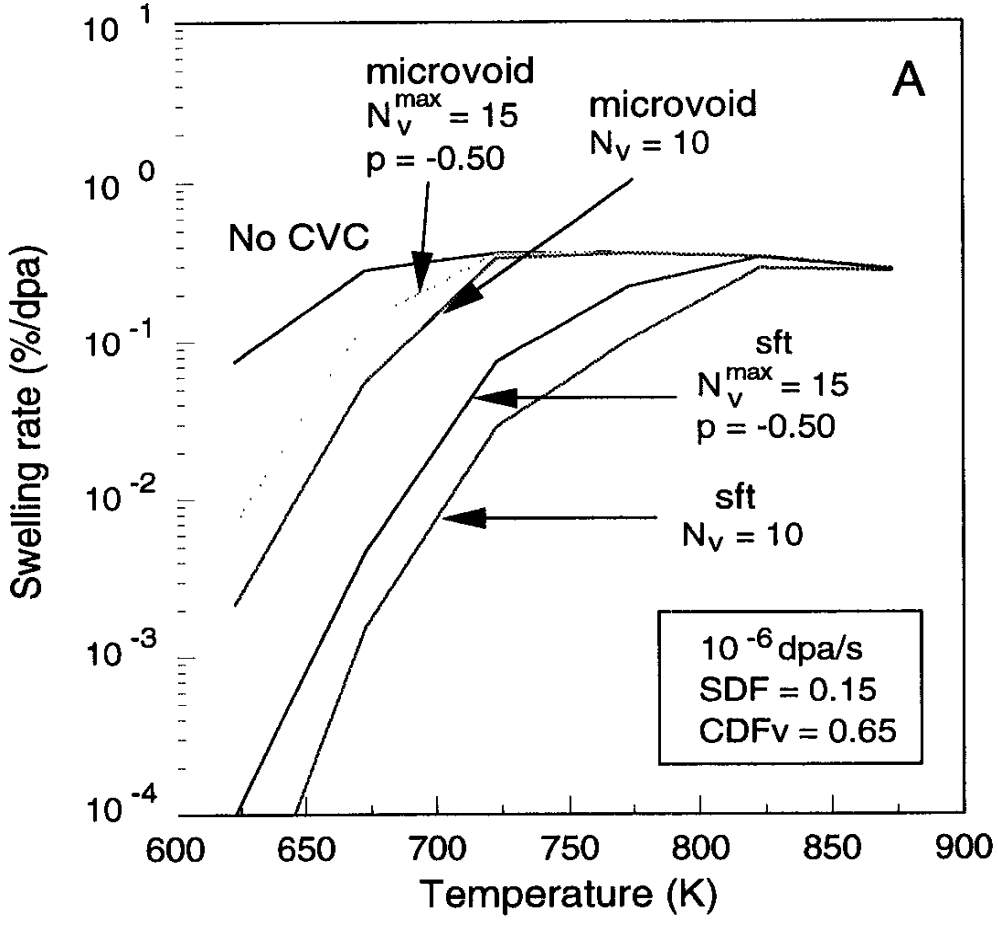

Fig. 6A - Influence of the initial size distribution of cascade vacancy clusters on swelling rate:: comparison of temperature dependence for the single-size case and the exponential function case.

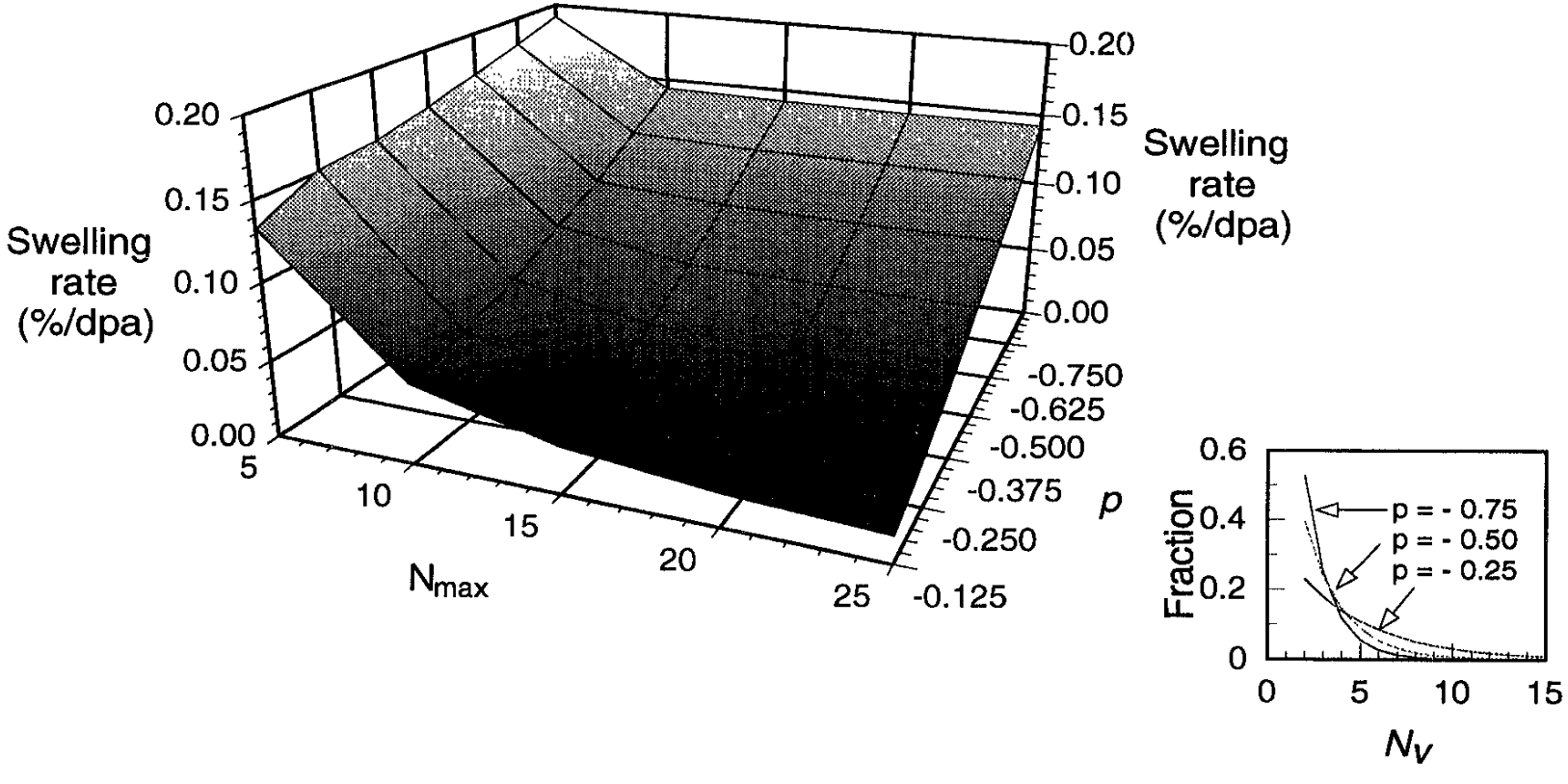

Fig. 6B - Influence of the initial size distribution of cascade vacancy clusters on swelling rate: dependence of swelling rate at 723K on the maximum cascade-cluster size Nmax and the exponent p. The inset shows the influence of p on the size distribution of the clusters.

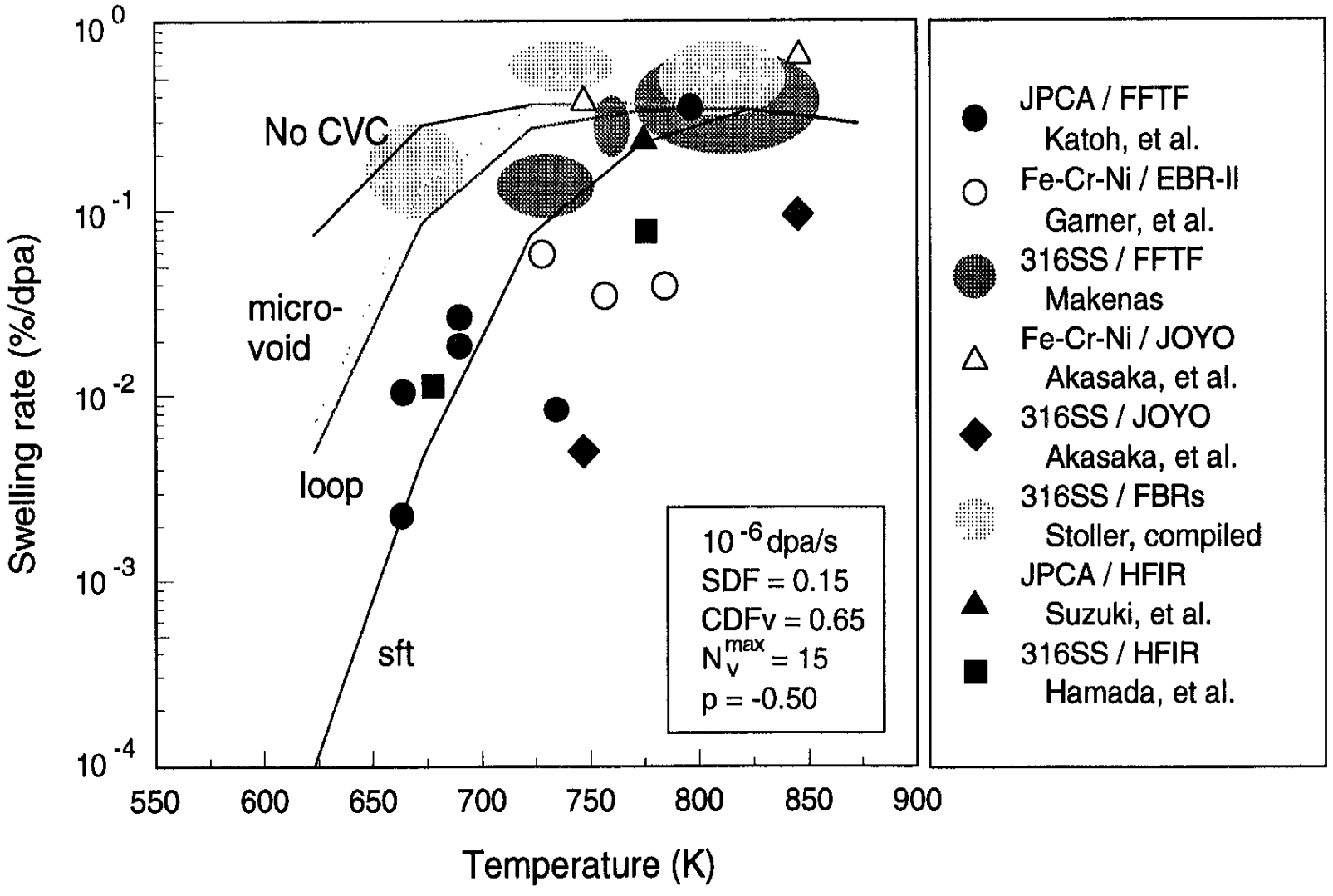

Fig. 7 - Temperature dependence of swelling rate under typical heavily irradiated microstructural conditions in austenitic stainless steels; comparison of computational results and experimental data.

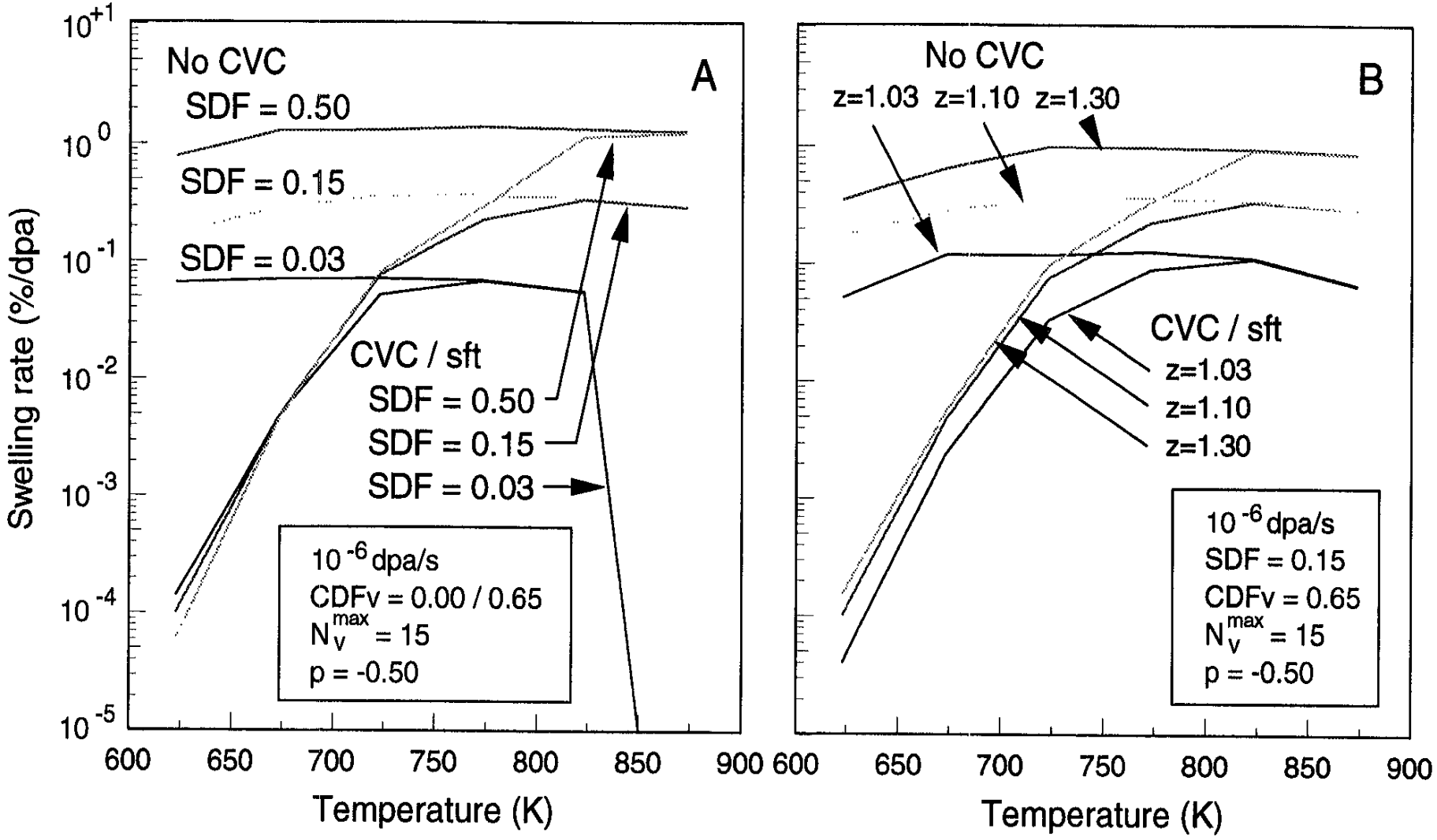

Fig. 8 - Influence of surviving defect fraction (A) and dislocation-interstitial bias factor (B) on temperature dependence of swelling rates with or withoutcascade vacancy cluster production. Vacancy cluster configuration was assumed to be stacking fault tetrahedron.

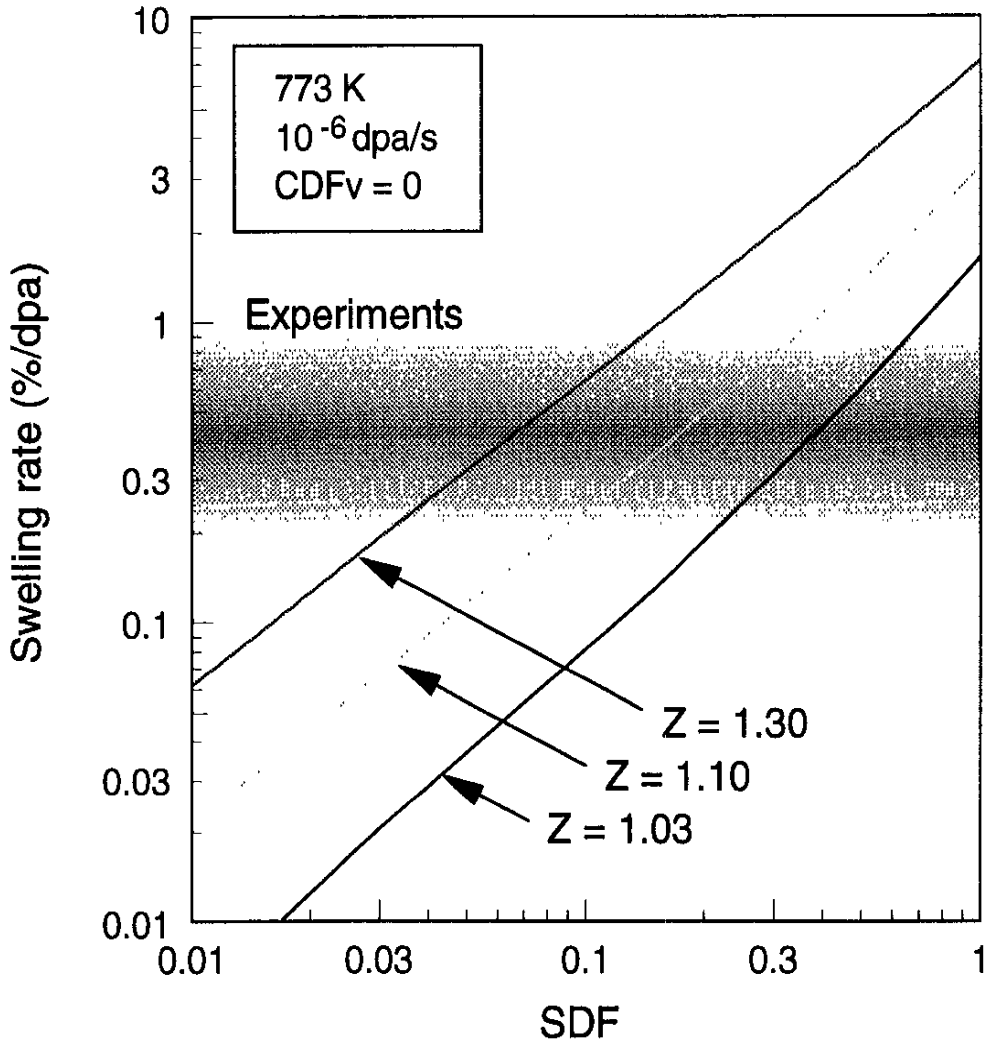

Fig. 9 - Effect of surviving defect fraction on swelling rate, at various dislocation - interstitial bias factors, under a microstructural condition typical in austenitic stainless steels heavily irradiated at 773K. A comparison to experimental data band suggests that a realistic range of surviving defect fraction roughly falls between 0.05 and 0.3.

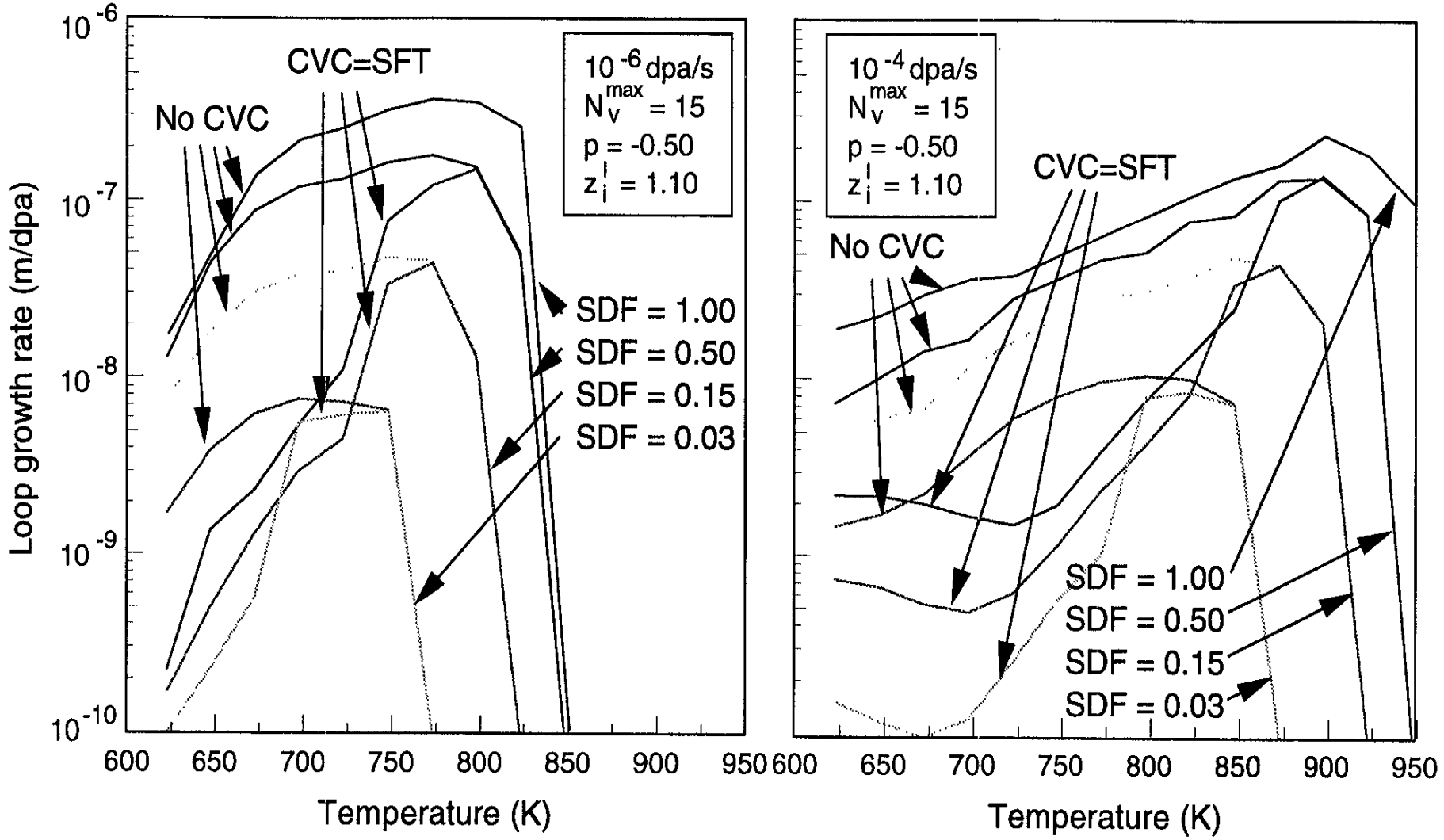

Fig. 10 - Influence of surviving defect fraction and cascade vacancy cluster production on radial growth rates of Frank dislocation loops. Clustered vacancy fraction of 0.65 was chosen when the production of cascade vacancy clusters as stacking fault tetrahedra was assumed.

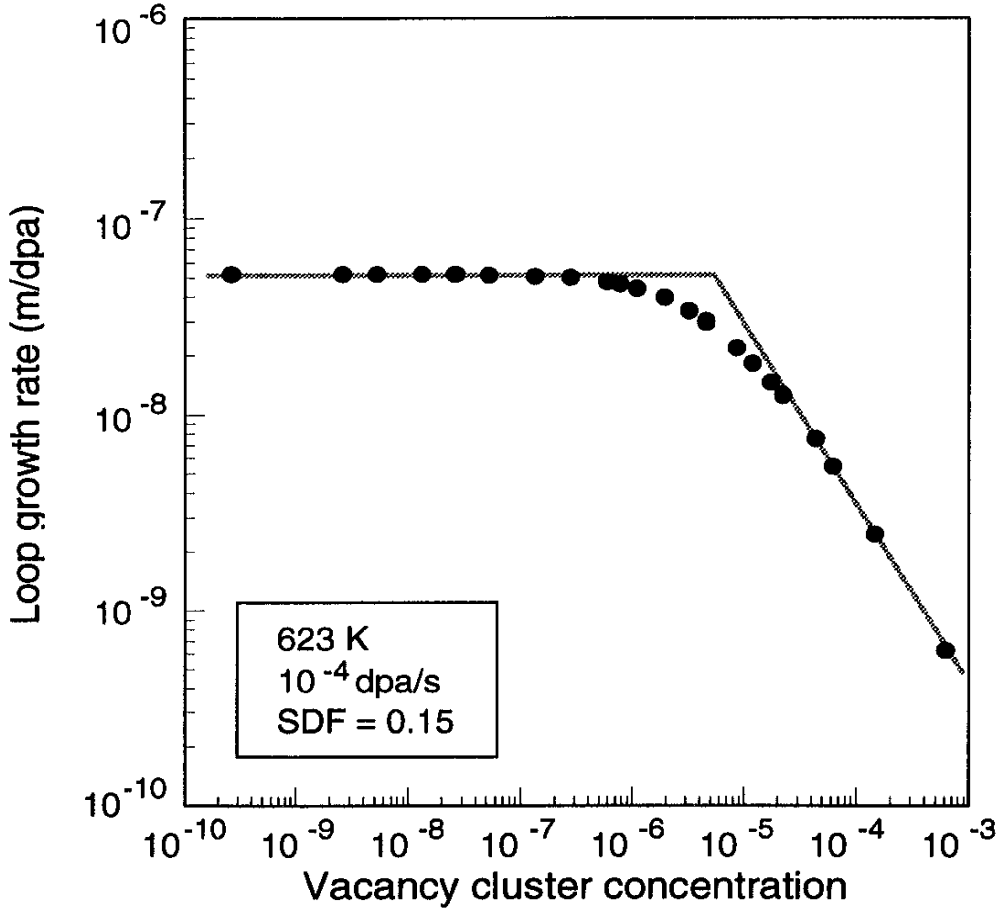

Fig. 11 - An example of relationship between Frank loop growth rate and vacancy cluster concentration. Vacancy clusters were assumed to be stacking fault tetrahedra.

Recent Issues of NIFS Series

NIFS-338 Y. Takeiri, A. Ando, O. Kaneko, Y. Oka, K. Tsumori, R. Akiyama, E. Asano, T. Kawamoto, M. Tanaka and T. Kuroda,
High-Energy Acceleration of an Intense Negative Ion Beam; Feb. 1995

NIFS-339 K. Toi, T. Morisaki, S. Sakakibara, S. Ohdachi, T.Minami, S. Morita, H. Yamada, K. Tanaka, K. Ida, S. Okamura, A. Ejiri, H. Iguchi, K. Nishimura, K. Matsuoka, A. Ando, J. Xu, I. Yamada, K. Narihara, R. Akiyama, H. Idei, S. Kubo, T. Ozaki, C. Takahashi, K. Tsumori,
H-Mode Study in CHS; Feb. 1995

NIFS-340 T. Okada and H. Tazawa,
Filamentation Instability in a Light Ion Beam-plasma System with External Magnetic Field; Feb. 1995

NIFS-341 T. Watanbe, G. Gnudi,
A New Algorithm for Differential-Algebraic Equations Based on HIDM; Feb. 13, 1995

NIFS-342 Y. Nejoh,
New Stationary Solutions of the Nonlinear Drift Wave Equation; Feb. 1995

NIFS-343 A. Ejiri, S. Sakakibara and K. Kawahata,
Signal Based Mixing Analysis for the Magnetohydrodynamic Mode Reconstruction from Homodyne Microwave Reflectometry; Mar.. 1995

NIFS-344 B.B.Kadomtsev, K. Itoh, S.-I. Itoh
Fast Change in Core Transport after L-H Transition; Mar. 1995

NIFS-345 W.X. Wang, M. Okamoto, N. Nakajima and S. Murakami,
An Accurate Nonlinear Monte Carlo Collision Operator; Mar. 1995

NIFS-346 S. Sasaki, S. Takamura, S. Masuzaki, S. Watanabe, T. Kato, K. Kadota,
Helium I Line Intensity Ratios in a Plasma for the Diagnostics of Fusion Edge Plasmas; Mar. 1995

NIFS-347 M. Osakabe,
Measurement of Neutron Energy on D-T Fusion Plasma Experiments; Apr. 1995

NIFS-348 M. Sita Janaki, M.R. Gupta and Brahmananda Dasgupta,
Adiabatic Electron Acceleration in a Cnoidal Wave; Apr. 1995

NIFS-349 J. Xu, K. Ida and J. Fujita,
A Note for Pitch Angle Measurement of Magnetic Field in a Toroidal

Plasma Using Motional Stark Effect; Apr. 1995

NIFS-350 J. Uramoto,
Characteristics for Metal Plate Penetration of a Low Energy Negative Muonlike or Pionlike Particle Beam: Apr. 1995

NIFS-351 J. Uramoto,
An Estimation of Life Time for A Low Energy Negative Pionlike Particle Beam: Apr. 1995

NIFS-352 A. Taniike,
Energy Loss Mechanism of a Gold Ion Beam on a Tandem Acceleration System: May 1995

NIFS-353 A. Nishizawa, Y. Hamada, Y. Kawasumi and H. Iguchi,
Increase of Lifetime of Thallium Zeolite Ion Source for Single-Ended Accelerator: May 1995

NIFS-354 S. Murakami, N. Nakajima, S. Okamura and M. Okamoto,
Orbital Aspects of Reachable β Value in NBI Heated Heliotron/Torsatrons; May 1995

NIFS-355 H. Sugama and W. Horton,
Neoclassical and Anomalous Transport in Axisymmetric Toroidal Plasmas with Electrostatic Turbulence; May 1995

NIFS-356 N. Ohyabu
A New Boundary Control Scheme for Simultaneous Achievement of H-mode and Radiative Cooling (SHC Boundary); May 1995

NIFS-357 Y. Hamada, K.N. Sato, H. Sakakita, A. Nishizawa, Y. Kawasumi, R. Liang, K. Kawahata, A. Ejiri, K. Toi, K. Narihara, K. Sato, T. Seki, H. Iguchi, A. Fujisawa, K. Adachi, S. Hidekuma, S. Hirokura, K. Ida, M. Kojima, J. Koong, R. Kumazawa, H. Kuramoto, T. Minami,. M. Sasao, T. Tsuzuki, J.Xu, I. Yamada, and T. Watari,
Large Potential Change Induced by Pellet Injection in JIPP T-IIU Tokamak Plasmas; May 1995

NIFS-358 M. Ida and T. Yabe,
Implicit CIP (Cubic-Interpolated Propagation) Method in One Dimension; May 1995

NIFS-359 A. Kageyama, T. Sato and The Complexity Simulation Group,
Computer Has Solved A Historical Puzzle: Generation of Earth's Dipole Field; June 1995

NIFS-360 K. Itoh, S.-I. Itoh, M. Yagi and A. Fukuyama,
Dynamic Structure in Self-Sustained Turbulence; June 1995

NIFS-361 K. Kamada, H. Kinoshita and H. Takahashi,
Anomalous Heat Evolution of Deuteron Implanted Al on Electron Bombardment; June 1995

NIFS-362 V.D. Pustovitov,
Suppression of Pfirsch-schlüter Current by Vertical Magnetic Field in Stellarators; June 1995

NIFS-363 A. Ida, H. Sanuki and J. Todoroki
An Extended K-dV Equation for Nonlinear Magnetosonic Wave in a Multi-Ion Plasma; June 1995

NIFS-364 H. Sugama and W. Horton
Entropy Production and Onsager Symmetry in Neoclassical Transport Processes of Toroidal Plasmas; July 1995

NIFS-365 K. Itoh, S.-I. Itoh, A. Fukuyama and M. Yagi,
On the Minimum Circulating Power of Steady State Tokamaks; July 1995

NIFS-366 K. Itoh and Sanae-I. Itoh,
The Role of Electric Field in Confinement; July 1995

NIFS-367 F. Xiao and T. Yabe,
A Rational Function Based Scheme for Solving Advection Equation; July 1995

NIFS-368 Y. Takeiri, O. Kaneko, Y. Oka, K. Tsumori, E. Asano, R. Akiyama, T. Kawamoto and T. Kuroda,
Multi-Beamlet Focusing of Intense Negative Ion Beams by Aperture Displacement Technique; Aug. 1995

NIFS-369 A. Ando, Y. Takeiri, O. Kaneko, Y. Oka, K. Tsumori, E. Asano, T. Kawamoto, R. Akiyama and T. Kuroda,
Experiments of an Intense H- Ion Beam Acceleration; Aug. 1995

NIFS-370 M. Sasao, A. Taniike, I. Nomura, M. Wada, H. Yamaoka and M. Sato,
Development of Diagnostic Beams for Alpha Particle Measurement on ITER; Aug. 1995

NIFS-371 S. Yamaguchi, J. Yamamoto and O. Motojima;
A New Cable -in conduit Conductor Magnet with Insulated Strands; Sep. 1995

NIFS-372 H. Miura,
Enstrophy Generation in a Shock-Dominated Turbulence; Sep. 1995

NIFS-373 M. Natsir, A. Sagara, K. Tsuzuki, B. Tsuchiya, Y. Hasegawa, O. Motojima,
Control of Discharge Conditions to Reduce Hydrogen Content in Low Z

Films Produced with DC Glow; Sep. 1995

NIFS-374 K. Tsuzuki, M. Natsir, N. Inoue, A. Sagara, N. Noda, O. Motojima, T. Mochizuki, I. Fujita, T. Hino and T. Yamashina,
Behavior of Hydrogen Atoms in Boron Films during H_2 and He Glow Discharge and Thermal Desorption; Sep. 1995

NIFS-375 U. Stroth, M. Murakami, R.A. Dory, H. Yamada, S. Okamura, F. Sano and T. Obiki,
Energy Confinement Scaling from the International Stellarator Database; Sep. 1995

NIFS-376 S. Bazdenkov, T. Sato, K. Watanabe and The Complexity Simulation Group,
Multi-Scale Semi-Ideal Magnetohydrodynamics of a Tokamak Plasma; Sep. 1995

NIFS-377 J. Uramoto,
Extraction of Negative Pionlike Particles from a H2 or D2 Gas Discharge Plasma in Magnetic Field; Sep. 1995

NIFS-378 K. Akaishi,
Theoretical Consideration for the Outgassing Characteristics of an Unbaked Vacuum System; Oct. 1995

NIFS-379 H. Shimazu, S. Machida and M. Tanaka,
Macro-Particle Simulation of Collisionless Parallel Shocks; Oct. 1995

NIFS-380 N. Kondo and Y. Kondoh,
Eigenfunction Spectrum Analysis for Self-organization in Dissipative Solitons; Oct. 1995

NIFS-381 Y. Kondoh, M. Yoshizawa, A. Nakano and T. Yabe,
Self-organization of Two-dimensional Incompressible Viscous Flow in a Friction-free Box; Oct. 1995

NIFS-382 Y.N. Nejoh and H. Sanuki,
The Effects of the Beam and Ion Temperatures on Ion-Acoustic Waves in an Electron Beam-Plasma System; Oct. 1995

NIFS-383 K. Ichiguchi, O. Motojima, K. Yamazaki, N. Nakajima and M. Okamoto
Flexibility of LHD Configuration with Multi-Layer Helical Coils; Nov. 1995

NIFS-384 D. Biskamp, E. Schwarz and J.F. Drake,
Two-dimensional Electron Magnetohydrodynamic Turbulence; Nov. 1995

NIFS-385 H. Kitabata, T. Hayashi, T. Sato and Complexity Simulation Group,
Impulsive Nature in Collisional Driven Reconnection; Nov. 1995